# Optical Impedance Spectroscopy with Single-Mode Electro-Active-Integrated Optical Waveguides

Xue Han and Sergio B. Mendes*

Department of Physics and Astronomy, University of Louisville, Louisville, Kentucky 40292, United States

S *Supporting Information*

ABSTRACT: An optical impedance spectroscopy (OIS) technique based on a single-mode electro-active-integrated optical waveguide (EA-IOW) was developed to investigate electron-transfer processes of redox adsorbates. A highly sensitive single-mode EA-IOW device was used to optically follow the time-dependent faradaic current originated from a submonolayer of cytochrome *c* undergoing redox exchanges driven by a harmonic modulation of the electric potential at several dc bias potentials and at several frequencies. To properly retrieve the faradaic current density from the ac-modulated optical signal, we introduce here a mathematical formalism that (i) accounts for intrinsic changes that invariably occur in the optical baseline of the EA-IOW device during potential modulation and (ii) provides accurate results for the electro-chemical parameters. We are able to optically reconstruct the faradaic current density profile against the dc bias potential in the working electrode, identify the formal potential, and determine the energy-width of the electron-transfer process. In addition, by combining the optically reconstructed faradaic signal with simple electrical measurements of impedance across the whole electrochemical cell and the capacitance of the electric double-layer, we are able to determine the time-constant connected to the redox reaction of the adsorbed protein assembly. For cytochrome *c* directly immobilized onto the indium tin oxide (ITO) surface, we measured a reaction rate constant of 26.5 s^{-1}. Finally, we calculate the charge-transfer resistance and pseudocapacitance associated with the electron-transfer process and show that the frequency dependence of the redox reaction of the protein submonolayer follows as expected the electrical equivalent of an RC-series admittance diagram. Above all, we show here that OIS with single-mode EA-IOW's provide strong analytical signals that can be readily monitored even for small surface-densities of species involved in the redox process (e.g., fmol/cm^2, 0.1% of a full protein monolayer). This experimental approach, when combined with the analytical formalism described here, brings additional sensitivity, accuracy, and simplicity to electro-chemical analysis and is expected to become a useful tool in investigations of redox processes.
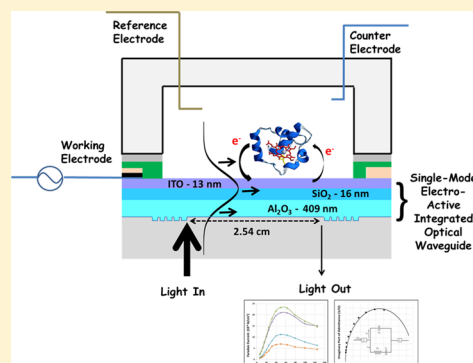
Characterizing, understanding, and controlling at a molecular level the structure and kinetics of electron-transfer process in molecular assemblies at electrode surfaces are crucial to several biological, chemical, and physical phenomena with important impacts in many technologies such as biosensing, catalysis, and organic electronics.[1] The determination of the electro-chemical faradaic current and the associated reaction rate constant by ac impedance spectroscopy, ac polarography, or ac voltammetry have been extensively reported in the literature. However, large electric double-layer capacitance and solution resistance make the determination of redox properties of an electro-chemically active submonolayer very difficult by those traditional electrochemical techniques.[2] Spectro-electrochemical methods, where an optical signal is spectrally tuned to probe exclusively the faradaic process, can potentially provide a superior route to investigate electron-transfer processes in molecular adsorbates by avoiding nonfaradaic components that typically hinders conventional electrochemical approaches using electrical signals alone.[2,3]

Niki and Sagara have developed an electro-reflectance (ER) technique[2,4] to study the kinetics of redox couples where an ac-modulation in the electric potential is applied to a thin-film

under investigation to drive the reflected optical signal from the sample. From measurements of the optical response at several modulation frequencies, it is then possible to determine the time response of the electron-transfer process. Fujishima and co-workers have implemented an analogous technique using transmittance measurements,[5] which is known as color impedance spectroscopy. However, those approaches use configurations with either a single-bounce in reflection or a single-pass in transmission on the sample of interest. As a consequence, the amplitude of the ac optical response is often too small to be detected either (i) for a redox couple with a small difference in their extinction coefficients or (ii) for molecular assemblies with low surface densities, or (iii) for an adsorbate with a low number of electro-chemically active species.

Saavedra, Doherty, Araci, and co-workers[6a−c] have successfully developed and applied a technique that enhances the
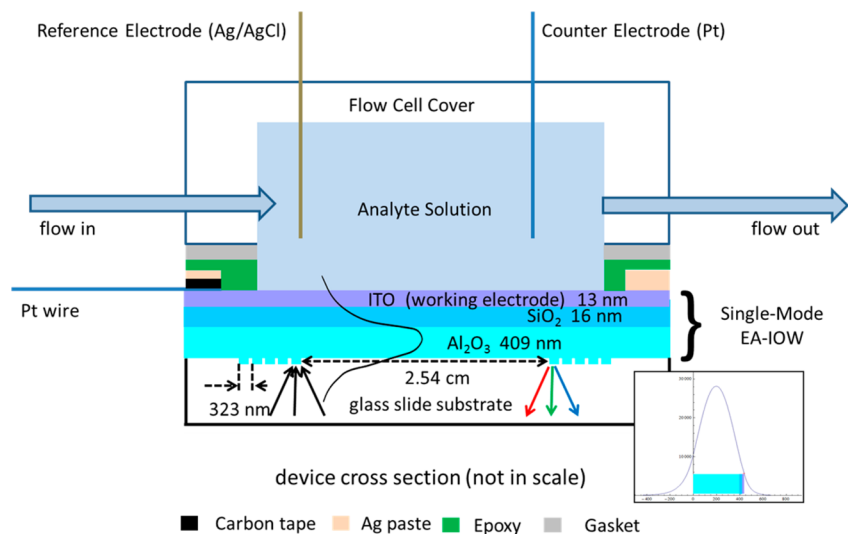
Figure 1. Schematic representation of the spectro-electrochemical cell (not to scale) with the multilayer structure of the single-mode EA-IOW structure. The inset shows the electromagnetic field distribution across the guiding structure for the TE polarization with the color bands representing each layer in the structure.

analytical signal by using an attenuated total reflectance geometry with multiple bounces to probe an adsorbed electro-active layer under potential modulation. The potential-modulated attenuated total reflectance (PM-ATR) platform in those works used thin glass slides with a thickness of either 1 mm or 150 μm as an internal reflection element. Those devices can then enhance the optical signal by about 35−100 compared to single-bounce reflectance or single-pass transmittance geometries. This enhancement in the analytical signal is usually termed as a sensitivity factor[7] and described by the variable S.

An integrated optical waveguide (IOW) can be considered as the ultimate limit of an ATR geometry where the thickness of the internal reflection element is reduced in order to increase the number of bounces on the analytical surface and enhance the sensitivity factor for probing surface-adsorbed species with the evanescent field. As the thickness of the guiding element gets smaller (in the order of the light wavelength), the discrete nature of the propagating guided modes must be considered for proper description of the optical phenomena. As shown elsewhere,[7a,8] the maximum sensitivity for probing surface-adsorbed species is reached for an IOW device with a tight confinement of the light beam that only one guided-mode is allowed to propagate along the IOW geometry; this geometry is known in literature as a single-mode IOW. Because of (i) the tight confinement of the guided light beam and (ii) the long path length of interaction between the surface-adsorbed species and the evanescent field of the propagating lightwave, the single-mode IOW has been demonstrated to reach values of the sensitivity factor, S, that are higher than 10 000 compared to single-bounce reflection or single-pass transmission geometries.[7a,8]

Previous work by Mendes, Saavedra, Armstrong, and co-workers[7a,9] have demonstrated the feasibility of performing spectro-electrochemistry with single-mode electro-active IOWs. An extremely thin layer of a transparent conducting electrode (ITO) deposited over a single-mode IOW has been shown to create an electro-active (EA) interface that could be used to study electro-chemically active adsorbates by measuring either (i) a monochromatic optical signal under a cyclic voltammetry (CV) scan or (ii) a broadband spectrum at specific electric

potentials. The present work benefits from those previous accomplishments and further develops the single-mode EA-IOW technology.

To enable extremely sensitive investigations on the kinetics and structure of electron-transfer processes of surface-adsorbed species, in this work we develop an optical impedance spectroscopy (OIS) technique that employs a single-mode electro-active integrated optical waveguide (EA-IOW) platform. The OIS approach is based on the application of an ac-modulated electric potential to drive the redox state of surface-adsorbed species and on the use of an optical signal guided along a single-mode EA-IOW to follow the time-dependent spectro-electrochemical event. Thus, OIS is a frequency-domain measurement of potential-modulated light absorption using a highly sensitive single-mode EA-IOW. In order to properly retrieve electro-chemical information from the modulated optical signal, a mathematical formalism is introduced here. Such formalism is required to account for intrinsic and systematic changes that invariably occur in the optical baseline of a single-mode EA-IOW device under potential modulation. Experimental optical data are then analyzed to reconstruct the faradaic process in a molecular adsorbate and determine several electro-chemical properties including the temporal response of the electron-transfer event as defined by the reaction rate constant.

The presentation of our work is organized in the following way. First, in Experimental Setup, we provide details of our device fabrication and experimental setup. Next, in Theory for OIS with EA-IOW, we establish a mathematical formalism to retrieve results of the electro-chemical process from the measured optical data in the general case when the optical baseline cannot be considered constant under potential modulation. Our analysis prescribes how the modulated optical signals obtained in the presence and in the absence of the redox adsorbate (including both dc and ac components) must be used to properly determine the optical absorbance related exclusively to the redox process. Next, we show how the ac-component of the modulated optical absorbance can be used to calculate the faradaic current density of surface-adsorbed redox species under interrogation. Then, we demonstrate that by combining the

faradaic current with simple measurements of the electric double-layer capacitance and the electrical impedance of the whole electro-chemical cell it is straightforward to determine the reaction rate constant associated with the electron-transfer process. In Experimental Results of OIS with EA-IOW, we report on experimental results that fully benefit from the developed analysis in the electro-chemical characterization of redox properties of a submonolayer of the cytochrome *c* protein adsorbed to an ITO surface.

■ EXPERIMENTAL SETUP

Single-Mode EA-IOW. The single-mode electro-active integrated optical waveguide employed in this work was formed by a three-layer stack of alumina (409 nm), silica (15 nm), and indium tin oxide (13 nm), as schematically shown in Figure 1. The electromagnetic mode-field profile of the multilayer integrated optical waveguide was calculated using a transfer-matrix method,[7a,10] and the results are displayed in the inset of Figure 1 for the TE polarization. In order to couple a light beam in and out of the EA-IOW device, a pair of surface-relief gratings were fabricated on a glass substrate, as reported by us elsewhere,[7b,11] prior to depositing the multilayer stack. When the surface-relief gratings (both with a pitch size of 323 nm in this work) are combined with highly anamorphic and large numerical aperture optics,[12] they enable broadband light (propagating in free space) to be coupled to the single-mode EA-IOW device. For the current experiments, the waveguide grating-couplers and associated optics were designed and fabricated to provide a spectral width of more than 100 nm centered at 530 nm. The separation between the two gratings, which defines the propagation length along the EA-IOW device, was set to 2.54 cm during device fabrication. After the grating fabrication, each glass substrate was coated with highly transparent alumina and silica layers using an atomic layer deposition (ALD) process as developed by our group.[13] The silica layer was included in the stack to protect the alumina layer from possible ion migration during the deposition and annealing of the ITO film. A pulsed dc sputtering technique was used to deposit the ITO layer. A careful calibration and optimization of the ITO deposition process was performed[14] to reach both high electrical conductivity (resistivity of about $\rho = 10^{-3}$ Ω cm) and high optical transparency (extinction coefficient of about 10^{-3}). In addition to the optimized deposition process, the EA-IOW device with its 13-nm ITO film was submitted to two annealing processes to improve its optical and electrical properties. One inert-annealing in nitrogen atmosphere at 250 °C and one reactive-annealing in room air at 100−150 °C were used to further optimize the ultrathin ITO film. After such procedures, a single-mode EA-IOW device with an attenuation loss of about 6 dB/cm loss and square resistance of about 2 KΩ/square (with a resistivity of $\rho = 3 \times 10^{-3}$ Ω cm) was achieved. The thickness of each layer in the fabricated device was determined by measuring the transmittance spectrum after the ALD and sputtering depositions and fitting those results with theoretical calculations[15] to find the optical constants and thickness of each layer. Accurate information on each layer thickness and refractive index are critical to calculate the sensitivity factor, *S*, defined as the absorbance measured by the EA-IOW device divided by the absorbance measured in a direct transmission configuration for an arbitrary but identical layer of chromophores.[7a,8] For the single-mode EA-IOW device described in Figure 1 in the spectral region of interest here (∼550 nm), we

calculated a sensitive factor of *S* = 14 428 at the transverse-electric (TE) polarization, which is very high due to the single-mode operation of the IOW and long propagation length (2.54 cm) along the device (see the Supporting Information for an experimental determination of the sensitivity factor). Such high sensitivity provides the possibility to detect molecular adsorbates with low surface densities (small fractions of a monolayer) and/or weak molar absorptivities.

Electrochemical Cell. Prior to its deployment, the fabricated single-mode EA-IOW device was initially incubated for at least 24 h in buffer solution (Na_2HPO_4, 5 mM, pH 7) in order to stabilize the ITO film. Then the device was removed from the solution, rinsed with DI water, dried out by blowing nitrogen gas, and set for electrical connections as indicated in Figure 1. To provide electrical contact to the potentiostat (CHI 660D), a platinum wire was fixed to the ITO working electrode surface by using a carbon tape. To ensure that the ITO film would provide about the same electric potential across its active surface, a thin layer of silver paste was placed on the periphery of the EA-IOW device (near but away from the optical path). An insulating epoxy layer was then used to cover the silver paste and prevent the silver metal to interact with the solution inside the electrochemical cell. A homemade Ag/AgCl pseudoreference electrode and a platinum counter-electrode were mounted in the flowcell just above the working ITO electrode. Our pseudoreference electrode showed an offset of (−0.085 ± 0.006) V with respect to a standard reference electrode of Ag/AgCl−1 M KCl (from CH Instruments, Inc.). All the electrical arrangements were made such that the light path between the two light-coupling gratings would not be disturbed during its operation. Each electrically wired EA-IOW device was then further stabilized inside the flowcell filled with buffer solution under CV modulation from −0.4 to 0.8 V using scanning rates of 0.20 V/s, 0.10 V/s, and 0.02 V/s.

Solutions of oxidized cytochrome *c* were prepared from horse heart, which was purchased from Sigma Aldrich with 99.7% purity and diluted to 100 nM in phosphate buffer solutions (Na_2HPO_4, 5 mM, pH 7). As a control experiment, one of the oxidized cytochrome *c* solutions was submitted to a chemically reducing agent and conventional spectrophotometric measurements confirmed that 100% of the dissolved species could be chemically reduced.

■ THEORY FOR OIS WITH EA-IOW

We start our theoretical analysis by describing the waveform of an electric potential with a sine wave modulation at an angular frequency ω:

$$E = E_{dc} + \Delta E_{ac} \sin(\omega t) \tag{1}$$

where E_{dc} represents the dc bias term and ΔE_{ac} represents the amplitude of an ac modulation. For small amplitudes of the potential modulation ($\Delta E_{ac} \ll (RT/nF)$, where R is the gas constant, T is the temperature, n is the number of electrons transferred in each redox event, and F is the Faraday constant), the output response described by the optical intensity propagating through the single-mode EA-IOW device can be expressed in the linear regime. Thus, the time-dependent optical response of the baseline signal can be described by

$$I_0 = I_{dc,0} + \Delta I_{ac,0} \sin(\omega t + \theta_0) \tag{2}$$

and the optical signal obtained when redox species are adsorbed to the analytical surface can be described similarly by
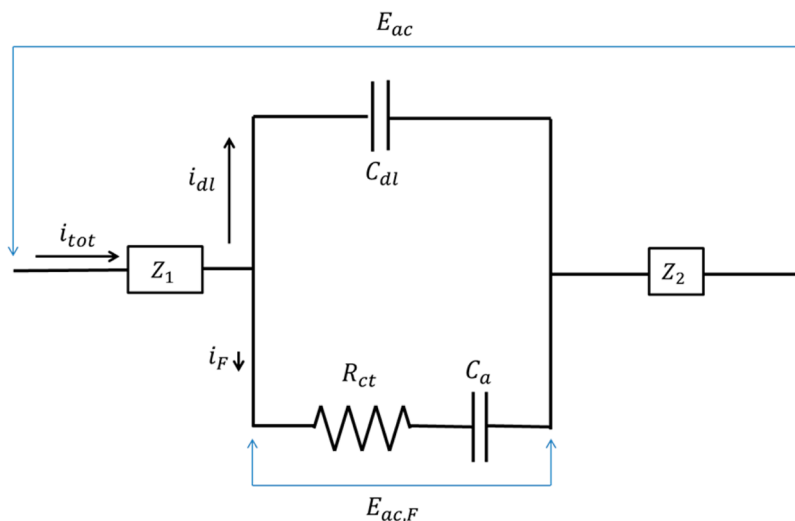
Figure 2. Electrical components of the electrochemical cell. The faradaic components are represented by R_{ct} and C_a, the electric-double layer capacitance is given by C_{dl}, Z_1 can account for the solution resistance, and Z_2 for an arbitrary additional electrical component.

$$I = I_{dc} + \Delta I_{ac} \sin(\omega t + \theta) \tag{3}$$

Those three waveforms (i.e., eqs 1−3) constitute the fundamental pieces of data to be collected from the experiment, and they form the basis from where all other outcomes will be derived. Obviously $I_{dc,0}$ and I_{dc} represent terms that are constants in time and their values will depend solely on E_{dc}. The terms $\Delta I_{ac,0}$ and ΔI_{ac} represent the amplitudes, and the terms θ_0 and θ represent the phases of the optical signal response originated under the electric potential modulation. In general, both amplitudes and phases are functions of E_{dc}, ΔE_{ac}, and ω. From the definition of absorbance and using eqs 2 and 3 we have

$$A \equiv -\log_{10}\left[\frac{I}{I_0}\right] = -\log_{10}\left[\frac{I_{dc}}{I_{dc,0}}\right] - \frac{\ln\left[1 + \frac{\Delta I_{ac}\sin(\omega t + \theta)}{I_{dc}}\right]}{\ln(10)}$$
$$+ \frac{\ln\left[1 + \frac{\Delta I_{ac,0}\sin(\omega t + \theta_0)}{I_{dc,0}}\right]}{\ln(10)} \tag{4}$$

Because $(nF\Delta E_{ac})/(RT) \ll 1$ then the terms $\Delta I_{ac}/I_{dc}$ and $\Delta I_{ac,0}/I_{dc,0}$ inside the natural logarithmic functions are small numbers and we can truncate the Taylor series expansion of those functions to the linear term and write

$$A \cong A_{dc} + \Delta A_{ac,in} \sin(\omega t) + \Delta A_{ac,out} \cos(\omega t)$$
$$= A_{dc} + \Delta A_{ac} \sin(\omega t + \delta_a) \tag{5}$$

where

$$A_{dc} \equiv -\log_{10}\left[\frac{I_{dc}}{I_{dc,0}}\right] \tag{6}$$

$$\Delta A_{ac,in} \equiv -\frac{\Delta I_{ac}\cos(\theta)}{I_{dc}\ln(10)} + \frac{\Delta I_{ac,0}\cos(\theta_0)}{I_{dc,0}\ln(10)} \tag{7}$$

$$\Delta A_{ac,out} \equiv -\frac{\Delta I_{ac}\sin(\theta)}{I_{dc}\ln(10)} + \frac{\Delta I_{ac,0}\sin(\theta_0)}{I_{dc,0}\ln(10)} \tag{8}$$

$$\Delta A_{ac} \equiv \sqrt{(\Delta A_{ac,in})^2 + (\Delta A_{ac,out})^2} \tag{9}$$

$$\delta_a \equiv \tan^{-1}\left(\frac{\Delta A_{ac,out}}{\Delta A_{ac,in}}\right) \tag{10}$$

Essentially, eq 5 prescribes that the absorbance response to an ac-potential modulation follows the standard pattern of a dc term, A_{dc}, and an ac-modulation term with an amplitude, ΔA_{ac}, and a phase, δ_a. Equations 7−10 instruct us on how to determine the amplitude and phase of the optical absorbance from quantities that are experimentally measured in response to the potential modulation. As seen in eqs 7 and 8, the ac components of the absorbance (both the in-phase and the out-of-phase components) depend on the difference between a measurement of the baseline and a measurement of the sample. Obviously, if the baseline is constant during the potential modulation, then $\Delta I_{ac,0} = 0$ and the baseline term vanishes, as assumed a priori in previous works of ER and PM-ATR.[6b,16] However, in general the baseline term can depend on the potential modulation and thus must be included in the measurements and calculations to reach proper results. We also observe in eqs 7 and 8 that in addition to the amplitudes of the ac terms, ΔI_{ac} and $\Delta I_{ac,0}$, one also needs to measure the dc terms, I_{dc} and $I_{dc,0}$, to perform the calculations of the ac-amplitude of the absorbance, ΔA_{ac}. Therefore, our experimental setup for the optical impedance spectroscopy to be described in Experimental Results of OIS with EA-IOW will consider provisions for those measurements.

Now, as we have determined the optical absorbance connected to the redox process, we aim to use such result to derive the associated faradaic current. We first notice that the faradaic current density, i_F, can be determined by the rate of change of surface-confined species undergoing redox exchanges, $d\Gamma/dt$, using the following expression:[2]

$$i_F = nF \frac{d\Gamma}{dt} \tag{11}$$

A key point in the analysis is that we can link the rate of change of surface-confined species undergoing redox exchanges, $d\Gamma/dt$, to the rate of change in the optical absorbance, dA/dt, by using

$$\frac{dA}{dt} = S \, \Delta \in \frac{d\Gamma}{dt} \qquad (12)$$

where S is the sensitivity factor of the single-mode EA-IOW device (as previously defined) and $\Delta \in$ is the change in molar absorptivity of the redox couple at the light wavelength. Then, by using eqs 11 and 12 and the time derivative of the absorbance from eq 5, we get

$$i_F = \frac{nF}{S \, \Delta \in} \frac{dA}{dt}$$

$$= i_{F,in} \sin(\omega t) + i_{F,out} \cos(\omega t)$$

$$= \Delta i_F \sin(\omega t + \delta_F) \qquad (13)$$

where

$$i_{F,in} \equiv -\frac{nF}{S \, \Delta \in} \omega \Delta A_{ac,out} \qquad (14)$$

$$i_{F,out} \equiv \frac{nF}{S \, \Delta \in} \omega \Delta A_{ac,in} \qquad (15)$$

$$\Delta i_F \equiv \sqrt{(i_{F,in})^2 + (i_{F,out})^2} = \frac{nF}{S \, \Delta \in} \omega \Delta A_{ac} \qquad (16)$$

$$\delta_F \equiv \tan^{-1}\left(\frac{\Delta i_{F,out}}{\Delta i_{F,in}}\right) = \delta_a + \frac{\pi}{2} \qquad (17)$$

And we can define in eq 16

$$\Delta \Gamma_{ac} \equiv \frac{\Delta A_{ac}}{S \, \Delta \in} \qquad (18)$$

which corresponds to the surface density of redox species participating in the electron-transfer process for a potential modulation of amplitude ΔE_{ac} at an angular frequency ω.

Up until now we have considered the output i_F (with its amplitude and phase) of the faradaic process in response to a potential modulation E_{ac} across the whole electrochemical cell, as schematically represented in Figure 2 with electrical components for the solution and electric double-layer, and equivalent electrical components for the electro-chemical redox process[2,6a] described by R_{ct} and C_a. Now, in order to specifically determine the time-response of the redox process and to factor out time-delay effects from other components in the electro-chemical cell, we need to relate the faradaic response i_F to a potential modulation imposed directly to the electron-transfer process, which is indicated in Figure 2 by the term described as $E_{ac,F}$. In other words, we need to find the admittance Y_F as defined by

$$Y_F \equiv \frac{I_F}{E_{ac,F}} \qquad (19)$$

where $I_F = i_F A_{eff}$ and A_{eff} is the effective electrode surface area involved in the faradaic process. But also from Figure 2, we can write

$$E_{ac,F} = \frac{I_F}{Y_F} = \frac{I_{dl}}{Y_{dl}} \qquad (20)$$

where I_{dl} and Y_{dl} are, respectively, the current and admittance associated with the electric double-layer component. The double-layer current, I_{dl}, can be written in terms of the total current I_t using $I_{dl} = I_t - I_F$, so we get

$$Y_F = \frac{Y_{dl}}{I_t - I_F} I_F \qquad (21)$$

But, as typically $I_F/I_t \ll 1$ (see the Supporting Information) then we can write

$$Y_F = \frac{Y_{dl}}{I_t} I_F = \frac{Y_{dl} Z_t I_F}{E_{ac}} \qquad (22)$$

where we have used $I_t = E_{ac}/Z_t$ with Z_t to represent the total electrical impedance measured across the whole electrochemical cell. Now, considering that the admittance of the electric double-layer admittance Y_{dl} can be written as $Y_{dl} = j\omega C_{dl}$, then we get

$$Y_F(\omega) = j\left(\frac{C_{dl} A_{eff}}{E_{ac}}\right) \omega Z_t(\omega) i_F(\omega) \qquad (23)$$

The admittance $Y_F(\omega)$ as calculated above describes the frequency dependence of the output response of the faradaic current to an input electric potential modulation of unit amplitude $E_{ac,F}$ applied directly to it. Now, considering that the faradaic process can be represented by an RC-series (specifically described by R_{ct} and C_a in Figure 2),[17] the admittance Y_F is then given by

$$Y_F(\omega) = \frac{R_{ct}}{\left(R_{ct}^2 + \frac{1}{\omega^2 C_a^2}\right)} + \frac{j}{\omega C_a \left(R_{ct}^2 + \frac{1}{\omega^2 C_a^2}\right)} \qquad (24)$$

And it is straightforward to calculate the derivative of the imaginary part of $Y_F(\omega)$ and show that

$$\frac{dY_{F,im}(\omega = \omega_r)}{d\omega} = 0 \qquad (25)$$

at the frequency

$$\omega = \omega_r \equiv \frac{1}{R_{ct} C_a} \qquad (26)$$

which is the resonant frequency of the faradaic process. Therefore, we can use the experimental data to determine the resonant frequency by employing the following relation:

$$\frac{dY_{F,im}(\omega)}{d\omega} = \frac{C_{dl} A_{eff}}{E_{ac}} \frac{d}{d\omega}\{Re[\omega Z_t(\omega) i_F(\omega)]\} = 0 \qquad (27)$$

We will find later that the approach of determining the resonant frequency by using the derivative of the imaginary part of the admittance, as described in eq 27, to be very useful (at least from an experimental perspective) because it only uses the angular frequency dependence present in the term: $Re[\omega Zt(\omega) i_F(\omega)]$, and it avoids possible experimental errors in the evaluation of the constants contained in the term $C_{dl} A_{eff}/\Delta E_{ac}$. Once the resonant frequency ω_r of the redox process has been determined we can then obtain the reaction rate constant[17] by the following expression:

$$K = \frac{\omega_r}{2} \qquad (28)$$

Also, at the resonant frequency, we notice from eqs 24 and 26 that

$$Y_F(\omega = \omega_r) = \frac{1}{2R_{ct}} + \frac{j}{2R_{ct}} = \frac{\omega_r C_a}{2} + \frac{j\omega_r C_a}{2} \qquad (29)$$
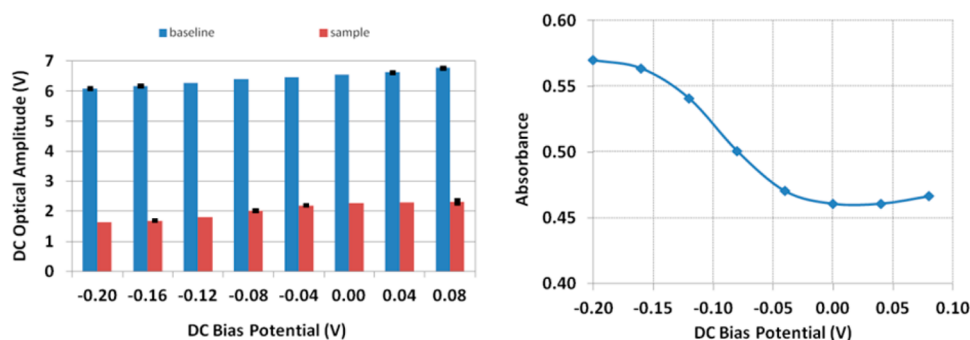
Figure 3. (a) dc component of the optical out-coupled intensities for the baseline and the cytochrome c adsorbed layer under ac potential modulation. (b) dc absorbance term, A_{dc}, at each dc bias potential.
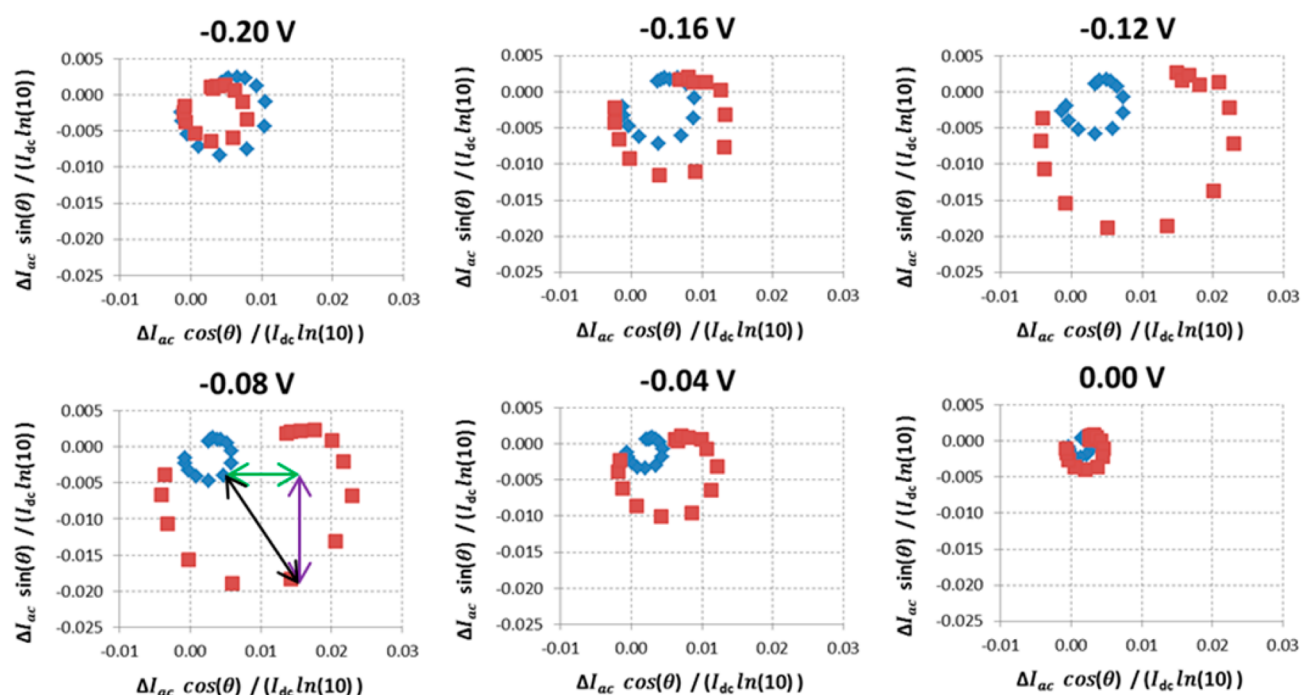

Figure 4. Schematic representation of the ac absorbance in the complex plane, where the $x-y$ coordinates correspond, respectively, to the in-phase and out-of-phase components of the optical signal shown in eqs 7 and 8. Blue diamond, data from the baseline measurement; red square, data measured with the adsorbed redox protein layer. Each point corresponds to a particular frequency, which increases clockwise from the smallest (1 Hz) to the largest (19.95 Hz). The distance between two points with the same frequency (black arrow) determines the amplitude of the ac absorbance term, ΔA_{ac}. The distance in the x-axis (green arrow) represents the in-phase component of the ac absorbance, $\Delta A_{ac,in}$. Likewise, the distance in the y-axis (purple arrow) corresponds to the out-of-phase component, $\Delta A_{ac,out}$.

which is useful to determine R_{ct} and C_a, after ω_r has been determined.

■ EXPERIMENTAL RESULTS OF OIS WITH EA-IOW

In this section, we apply the OIS technique with a single-mode EA-IOW device in order to characterize an electro-active adsorbate of cytochrome c species, and we demonstrate how the experimental data benefits from the previous theoretical analysis. For the experimental measurements, we employed an ac-modulation in the electric potential of $\Delta E_{ac} = 10$ mV (20 mV peak-to-peak) at several different dc bias potentials (E_{dc} from -0.20 V to $+0.08$ V) with a series of angular frequencies (ω from 2π rad/s to 40π rad/s). As the optical probing wavelength we utilized a spectral band centered at 550 nm with a full-width at half-maximum (fwhm) of 3 nm obtained from a supercontinuum laser source (FemtoPower 1060, Fianium Ultrafast Fiber Lasers) combined with an acousto-optical

tunable filter. The transverse electric (TE) polarization was selected for all experiments described in this work. The out-coupled signal from the EA-IOW was collected by a PMT (H5783, Hamamatsu) that was connected to a low-noise current preamplifier (SR570, Stanford Research Systems). An oscilloscope (DSO 8104A, Agilent) was used to simultaneously acquire the waveforms of the electric potential (originated by the potentiostat) and the optical signal response (provided by the current preamplifier). The electrical impedance across the electro-chemical cell as measured by the potentiostat was also recorded. Baseline signal (when no redox species were present in the flowcell) for each dc bias potential and each modulation frequency was measured first. Afterward, cytochrome c in buffer solution was injected into the flowcell, let it incubate for 30 min, and a similar sequence of measurements was applied. We note that, as the protein concentration in the solution phase was quite low (100 nM), the data above was collected without
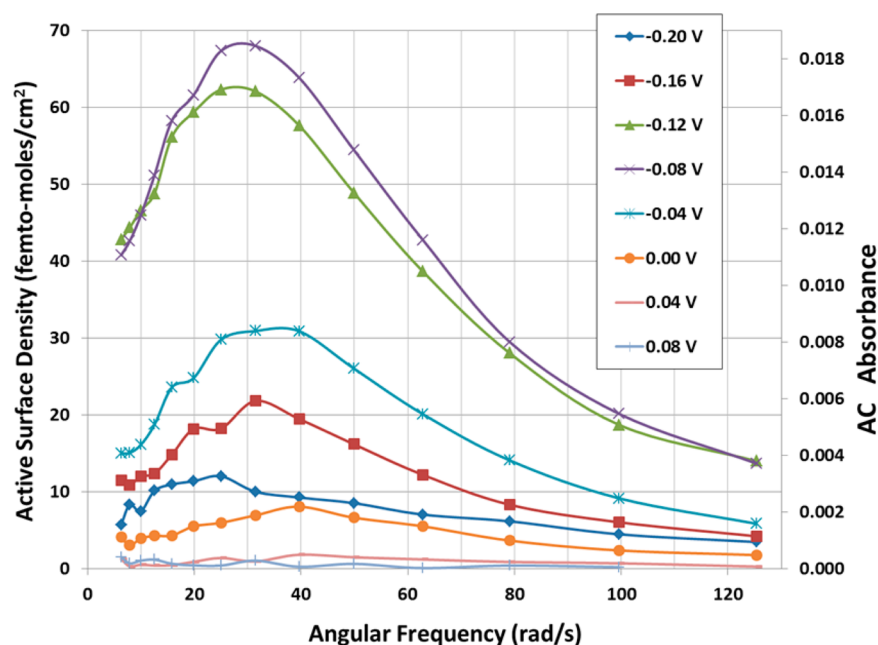
Figure 5. The *y*-axis on the right side displays the amplitude of the ac absorbance, ΔA_{ac}, against the angular frequency for an ac amplitude modulation of 10 mV in the electric potential at several dc bias potentials. The *y*-axis on the left side displays the corresponding surface density of cytochrome *c* molecules, $\Delta\Gamma_{ac}$, that are driven by the potential modulation.

rinsing the electrochemical cell. Preliminary data (not shown here) have demonstrated that the dissolved bulk phase species had no measurable impact on the results.

Results of dc Absorbance. Figure 3a shows at each dc bias potential the measured dc optical signals in the presence (red bars) and absence (blue bars) of the electro-active protein layer. The plot displays the average and error bar of the dc optical signals, which were calculated over the set of measured modulation frequencies. As expected, at a particular dc bias potential, the error bar is quite small indicating that the dc component of the optical response is independent of the modulation frequency. We also observe that the dc optical component of the baseline signal changes with the dc bias potential and it exhibits similar behavior as the baseline tested under a CV potential scan (data shown in Figure S.1b in the Supporting Information).

The dc absorbance term of the cytochrome *c* layer was calculated using eq 6, and the results are shown in Figure 3b. At the 550-nm wavelength, the molar absorptivity of cytochrome *c* at the two redox states[18] are $\in_{ox} = 9.0 \times 10^3$ M^{-1} cm^{-1} and $\in_{red} = 27.7 \times 10^{-3}$ M^{-1} cm^{-1} (which considered that the adsorption process does not significantly affect the protein molar absorptivity[19]). As we have initially injected oxidized cytochrome *c* into the flowcell and observed the absorbance to stabilize at a value of about 0.465 ± 0.003, we can then conclude that at positive values of the dc bias potential cytochrome molecules are fully oxidized with a total surface coverage of $\Gamma_{tot} = (A_{dc}(E_{dc} > 0 \text{ V}))/(S \in_{ox}) = 3.58 \pm 0.02$ pmol/cm^2, which corresponds to about 16% of a full monolayer (22 pmol/cm^2). Toward negative values of the dc bias potential, cytochrome *c* molecules start to reduce, and the redox process is observed to reach a plateau for values of the dc bias potential smaller than −0.16 V. Again, by using the measured dc absorbance (and considering no desorption/adsorption under potential modulation, as demonstrated in the Supporting Information) we have found that 11% of the

adsorbed species (0.39 pmol/cm^2) were electrically reduced as the dc bias potential was driven to negative values.

Results of ac Absorbance. The experimental data for the ac optical intensity collected under potential modulation at several frequencies and several dc bias potentials are schematically summarized in the complex plane shown in Figure 4.

Each plot shows data measured for both the baseline (blue diamonds) and when the redox-active layer is present (red squares). The amplitude of the ac absorbance, ΔA_{ac}, is mathematically described (see eqs 7 and 8) by the distance between two points with the same frequency, as schematically illustrated by the black arrow at the −0.08 V plot. The horizontal distance between those two points (green arrow) corresponds to the in-phase component of the ac absorbance, $\Delta A_{ac,in}$, and the vertical distance corresponds to the out-of-phase component, $\Delta A_{ac,out}$. As we can observe in the plots of Figure 4, the contributions from the baseline (blue diamonds) are not negligible and its magnitude changes as we apply different dc bias potentials and/or different modulation frequencies. As we already pointed out, their contribution must be considered for accurate results. From a general inspection of the plots in Figure 4, we can qualitatively conclude that the ac-amplitude of the absorbance reaches a maximum for a dc bias potential in the vicinity of −0.12 V and −0.08 V. A more quantitative statement of this observation can be found in Figure 5, where we have used eqs 7−9 to plot the ac-amplitude of the absorbance, ΔA_{ac} (the *y*-axis on the right side of the plot in Figure 5), against the angular frequency in the *x*-axis at different dc bias potentials. We observe a maximum AC absorbance of about $\Delta A_{ac} = 0.0183$ at $E_{dc} = -0.08$ V. We can confirm the consistency of this result by comparing it to the previous dc absorbance measurements. In Figure 3b, we note that the dc component of the absorbance has a maximum slope of $dA/dE \cong 0.877$ V^{-1} (at $E_{dc} = -0.08$ V). Now, for a peak-to-peak swing in the potential of 0.02 V ($\Delta E_{ac} = 10$ mV), one would expect from these results an absorbance change of $\Delta A = 0.0175$, which agrees remarkably
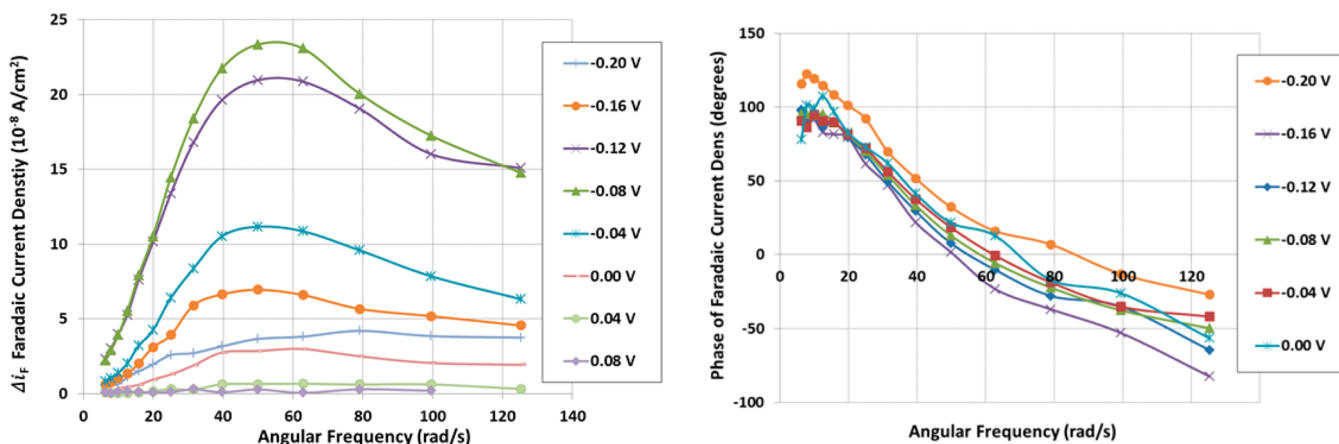
Figure 6. Faradaic current density versus angular frequency for a potential modulation of 10-mV amplitude at several dc bias potentials (a) ac amplitude and (b) phase.

well with the results from the ac measurements (ΔA_{ac} = 0.0183).

We then apply our previous relation, $\Delta \Gamma_{ac} = \Delta A_{ac}/S \Delta \in$, to obtain the amount of cytochrome c molecules engaged in the electron-transfer process under the ac potential modulation. In Figure 5, the y-axis on the left side shows $\Delta \Gamma_{ac}$ against the angular frequency for each dc bias potential. At the dc bias potential of -0.08 V, a maximum of 68 fmol/cm^2 of active cytochrome c responded to the ac potential oscillation. As the dc bias potential moves away from the formal potential, we observe as expected that the number of species involved in the redox process decreases. It is important to notice that the ability to detect such small amounts of species participating in the redox process is a direct consequence of the high sensitivity provided by the single-mode EA-IOW device.

Electro-Chemical Results. Next, we apply eqs 13−17 to determine the amplitude Δi_F and phase δ_F of the faradaic current density. Those results are shown in Figure 6a,b, where the faradaic process is plotted against the angular frequency at several dc bias potentials. At the lower end of the angular frequency spectrum, the amplitude of the faradaic current shows a linear behavior with a higher slope for those dc bias potentials that are closer to the formal potential.

Because it provides the maximum amplitude of the faradaic current, we now consider the angular frequency of $\omega = 49.9$ rad s^{-1}. We use the experimental data at this particular angular frequency to plot the amplitude of the faradaic current density Δi_F against the dc bias potential. Those experimental results are summarized in Figure 7. A Gaussian fit of the experimental data allow us to determine the formal potential at $E^0 = (-0.094 \pm 0.002)$ V with a fwhm of $\Delta E_{1/2} = (0.097 \pm 0.006)$ V. Taking into account the offset in our pseudoreference electrode, we determine a formal potential for cytochrome c adsorbed to the ITO surface of -0.012 V against a Ag/AgCl electrode, which is consistent with reported data.[20]

Information on the apparent number of electrons n_a involved in the redox process[2] can then be obtained from $n_a = 0.0906$ V/$\Delta E_{1/2}$. So, n_a is very close to 1 (0.93) indicating that the interaction between adsorbed cytochrome c molecules is weak, as one would expect due to the extremely low surface-density.

Electron-Transfer Rate Constant. To determine the reaction rate constant, we combine the data on the faradaic current, $i_F(\omega)$, described above with electrical measurements of the impedance across the electro-chemical cell, $Z_t(\omega)$, and the
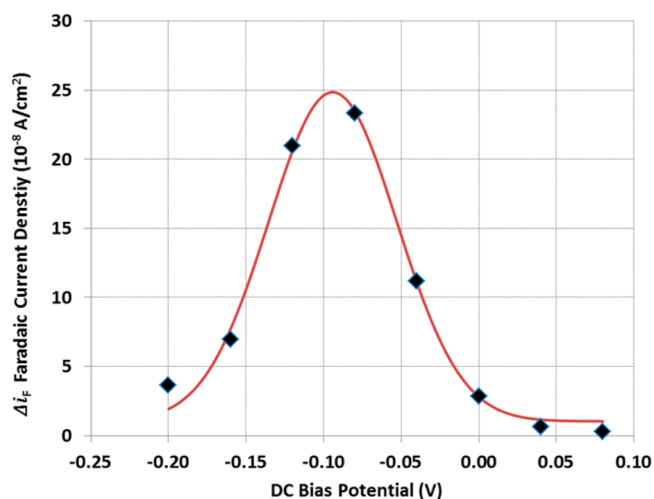

Figure 7. Black diamonds: experimental data for the faradaic current density versus dc bias potential at the angular frequency of 49.9 rad/s. Red curve, a Gaussian fitting curve that gave the following results: formal potential $E^0 = (-0.094 \pm 0.002)$ V with fwhm $\Delta E_{1/2} = (0.097 \pm 0.006)$ V.

capacitance of the electric double-layer capacitance, C_{dl}. Those conventional electrical measurements are described in the Supporting Information. We also determined the ITO area in our EA-IOW that was electrically active to be about $A_{eff} = 7.1$ cm^2. Then, with those measurements in hand, we used eq 23 to determine the admittance of the redox process. In Figure 8a we plot the imaginary part of the admittance against the modulation frequency. As described earlier, the angular frequency where the derivative of imaginary part of the admittance, $dY_{F,im}(\omega)/d\omega$, vanishes corresponds to the resonance frequency of the associated RC-series of the electron-transfer reaction. We used the experimental results summarized in Figure 8a to find a value of $\omega_r = 53$ rad/s for the resonant frequency. As we pointed earlier, this procedure for determining ω_r is immune to any experimental error in the evaluation of C_{dl} and A_{eff}, which is certainly relevant because we can then reach better accuracy in determining the reaction rate constant, which is given by eq 28. Our result of $K = 26.5$ s^{-1} for the reaction rate of cytochrome c adsorbed to an ITO surface under our particular aqueous buffer environment is consistent with previous work[21] in this field.
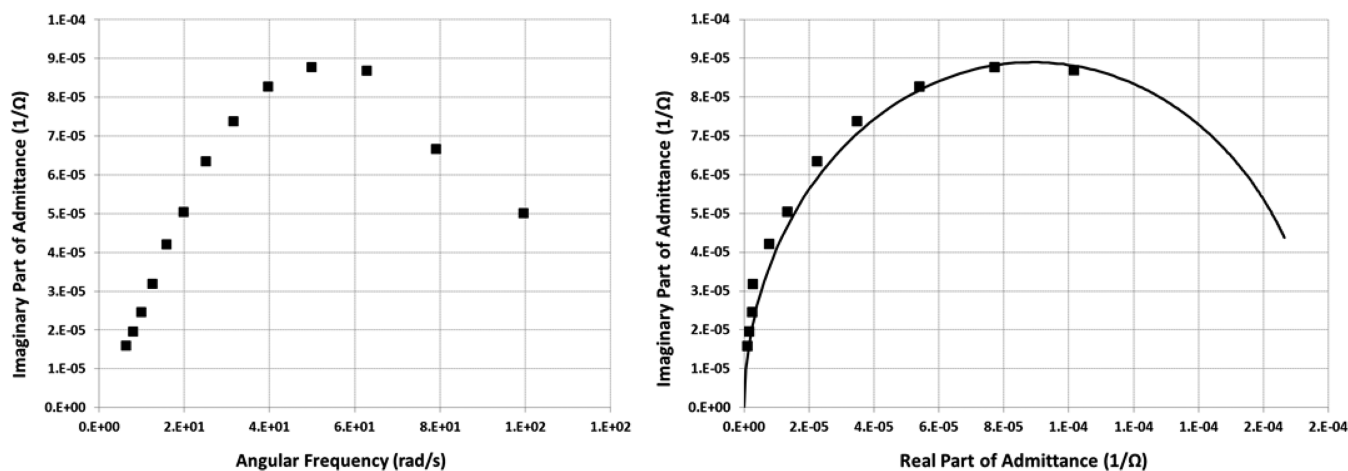
Figure 8. (a) Imaginary part of the impedance, $Y_{F,im}$, as described by eq 23. (b) Complex plane representation of the faradaic impedance Y_F: dots correspond to experimental data from eq 23, solid line corresponds to theoretical results from eq 24 based on a RC-series model for the electro-active protein assembly described by R_{ct} and C_a.

Next, we used the obtained value of ω_r and eq 29 to determine the value of the charge transfer resistance and pseudocapacitance associated with the redox process. Our findings for those quantities were R_{ct} = 5.62 KΩ and C_a = 3.35 μF. We then utilized those R_{ct} and C_a values to calculate the Nyquist diagram at several angular frequencies of an $R_{ct}C_a$-series admittance as determined by eq 24. In Figure 8b those calculated results are represented by the continuous solid line, and the measured experimental data are represented by the discrete squares. We observe a strong agreement among those results that corroborates the original assumption of an equivalent electrical circuit formed by the resistor-capacitor components in series to describe the chemical electron-transfer process.

Finally, we would like to mention that, as described in our theory Theory for OIS with EA-IOW, we have quantitatively taken into consideration the fact that $E_{ac,F}$ applied to the faradaic unit is different from E_{ac} applied to the working electrode. A similar consideration but using different approaches has been previously reported in the literature by other research groups (e.g., Gaigalas,[22] Finklea,[23] Sagara,[24] and Ohtsuka[25]). These approaches mainly use the uncompensated resistance to calculate $E_{ac,F}$. Among the merits of such approaches include the fact that (i) the uncompensated resistance has a value that is frequency- and potential-independent and (ii) the uncompensated resistance can be measured with high accuracy. In this work, we have used the condition that $I_F \ll I_t$, which combined with a constant capacitance for the electric double-layer C_{dl}, allowed us to derive a simple methodology for the determination of the reaction rate constant. Because such conditions were satisfied in our experiments, we were able to exploit several benefits from them: (i) the derivation of the faradaic admittance, eq 23, does not require any additional information about the electro-chemical cell beyond what has already been described in Figure 2; no additional model or value for a specific electric component was required and (ii) the total electrical impedance of the cell Z_t was measured directly through the electrical data collected by a potentiostat for every angular frequency in the experiment (see Figure S.3 in the Supporting Information) and those measurements automatically included the effects of any electrical component (for instance, those generically described by Z_1 and Z_2 in Figure 2) regardless of their nature or specific

characteristics, (iii) the experimental measurements for Z_t and I_F were performed simultaneously and under exactly the same working conditions. Those benefits were valuable to reach good agreement between the experimental data and theoretical calculations shown in Figure 8b. However, it is quite possible that under certain experimental conditions the requirements above may not be satisfied and the approaches already reported in the literature (and referenced above) may provide an alternative for extracting the aimed information on the reaction rate constant from our optically reconstructed faradaic current using the single-mode EA-IOW platform.

CONCLUSIONS

In this work we developed an optical impedance spectroscopy technique that uses a highly sensitive, single-mode, electro-active integrated optical waveguide to investigate electro-chemical properties of surface-bound redox species. The experimental results show that even for small surface-densities of species involved in the redox process (e.g., fmol/cm^2) our approach provides strong analytical signals that can be readily monitored and analyzed. The optically reconstructed faradaic process allowed us to determine several electro-chemical properties of a redox process in a molecular adsorbate including the temporal response of the electro-chemical process as defined by the reaction rate constant. The mathematical formalism and experimental methodology, which was put forward here to address data measured in the single-mode EA-IOW device, can also be applied to other configurations (e.g., ER, PM-ATR) and may potentially be helpful in these approaches as well. The outstanding sensitivity provided by the single-mode EA-IOW is expected to help in studies of redox couples with small differences in their extinction coefficients, molecular assemblies with low surface densities, or adsorbates with a low number of electro-chemically active species. The OIS using a single-mode EA-IOW combined with the analytical formalism described here brings additional sensitivity, accuracy, and simplicity to electro-chemical analysis and is expected to become a useful tool in investigations of redox processes.

■ ASSOCIATED CONTENT

Ⓢ Supporting Information

CV potential scans are reported on the optical baseline of the single-mode EA-IOW device to confirm the systematic changes already reported here under ac potential modulation, optical absorbance data reported to confirm the constancy of the surface-density of redox species under potential modulation, experimental data for measurements of the electrical impedance across the electro-chemical cell and the capacitance of the electric double-layer capacitance, and experimental data to independently quantify the sensitivity factor. This material is available free of charge via the Internet at http://pubs.acs.org.

■ AUTHOR INFORMATION

Corresponding Author
*E-mail: sbmend01@louisville.edu.

Notes
The authors declare no competing financial interest.

■ ACKNOWLEDGMENTS

■ REFERENCES

(1) (a) Dimitrakopoulos, C. D.; Malenfant, P. R. L. *Adv. Mater.* **2002**, *14* (2), 99. (b) Forrest, S. R. *Nature* **2004**, *428* (6986), 911−918. (c) Katz, E.; Willner, I. *Electroanalysis* **2003**, *15* (11), 913−947.

(2) Feng, Z. Q.; Sagara, T.; Niki, K. *Anal. Chem.* **1995**, *67* (19), 3564−3570.

(3) (a) Kuwana, T.; Winograd, N. In *Electroanalytical Chemistry*; Bard, A., Ed. Dekker: New York, 1974; Vol. 7, pp 1−78. (b) Heineman, W. R.; Hawkridge, F. M.; Blount, H. N. In *Electroanalytical Chemistry*; Bard, A., Ed. Dekker: New York, 1984; Vol. *13*, pp 1−113.

(4) Sagara, T.; Igarashi, S.; Sato, H.; Niki, K. *Langmuir* **1991**, *7* (5), 1005−1012.

(5) (a) Amemiya, T.; Hashimoto, K.; Fujishima, A. *Denki Kagaku* **1992**, *60* (12), 1075−1081. (b) Amemiya, T.; Hashimoto, K.; Fujishima, A. *J. Phys. Chem.* **1993**, *97* (38), 9736−9740. (c) Amemiya, T.; Hashimoto, K.; Fujishima, A. *J. Electroanal. Chem.* **1994**, *377* (1−2), 143−148. (d) Amemiya, T.; Hashimoto, K.; Fujishima, A.; Itoh, K. *J. Electrochem. Soc.* **1991**, *138* (10), 2845−2859.

(6) (a) Araci, Z. O.; Runge, A. F.; Doherty, W. J.; Saavedra, S. S. *Israel J. Chem.* **2006**, *46* (3), 249−255. (b) Doherty, W. J.; Wysocki, R. J.; Armstrong, N. R.; Saavedra, S. S. *J. Phys. Chem. B* **2006**, *110* (10), 4900−4907. (c) Araci, Z. O.; Shallcross, C. R.; Armstrong, N. R.; Saavedra, S. S. *J. Phys. Chem. Lett.* **2010**, *1* (12), 1900−1905.

(7) (a) Mendes, S. B., Saavedra, S. S.; Armstrong N. R. In *Optical Guided-Wave Chemical and Biosensors*, Zourob, M., Lakhtakia A., Eds.; Springer: Heidelberg, Germany, 2010. (b) Wiederkehr, R. S.; Hoops, G. C.; Mendes, S. B. *Opt. Eng.* **2011**, *50* (7), 071109.

(8) (a) Mendes, S. B.; Li, L. F.; Burke, J. J.; Lee, J. E.; Dunphy, D. R.; Saavedra, S. S. *Langmuir* **1996**, *12* (14), 3374−3376. (b) Mendes, S. B.; Saavedra, S. S. *Opt. Express* **1999**, *4* (11), 449−456.

(9) (a) Dunphy, D. R.; Mendes, S. B.; Saavedra, S. S.; Armstrong, N. R. *Anal. Chem.* **1997**, *69* (15), 3086−3094. (b) Dunphy, D. R.; Mendes, S. B.; Saavedra, S. S.; Armstrong, N. R. *Interfacial Electrochemistry*; Wieckowski, A., Ed.; Marcel Dekker: New York, 1999; Chapter 29. (c) Bradshaw, J. T.; Mendes, S. B.; Armstrong, N. R.; Saavedra, S. S. *Anal. Chem.* **2003**, *75* (5), 1080−1088.

(10) Offersgaard, J. F. *J. Opt. Soc. Am. A* **1995**, *12* (10), 7.

(11) Hayes, C. M.; Pereira, M. B.; Brangers, B. C.; Aslan, M. M.; Wiederkehr, R. S.; Lake, J. H.; Mendes, S. B. *17th Biennial University/Government/Industry Micro-Nano Symposium* **2008**, 227−232.

(12) Pereira, M. B.; Craven, J. S.; Mendes, S. B. *Opt. Eng.* **2010**, *49* (12).

(13) Aslan, M. M.; Webster, N. A.; Byard, C. L.; Pereira, M. B.; Hayes, C. M.; Wiederkehr, R. S.; Mendes, S. B. *Thin Solid Films* **2010**, *518* (17), 4935−4940.

(14) Han, X.; Mendes, S. B. *SPIE Optics and Photonics*, San Diego, CA, August 12−16, 2012.

(15) Macleod, H. A. *Thin-Film Optical Filters*, 2nd ed.; Macmillan Pub. Co.: New York, 1986.

(16) Feng, Z. Q.; Imabayashi, S.; Kakiuchi, T.; Niki, K. *J. Electroanal. Chem.* **1996**, *408* (1−2), 15−20.

(17) (a) Lelievre, D.; Plichon, V.; Laviron, E. *J. Electroanal. Chem.* **1980**, *112* (1), 137−145. (b) Laviron, E. *J. Electroanal. Chem.* **1979**, *97* (2), 135−149.

(18) Margoliash, E.; Frohwirt, N. *Biochem. J.* **1959**, *71* (3), 570−572.

(19) Wiederkehr, R. S.; Hoops, G. C.; Aslan, M. M.; Byard, C. L.; Mendes, S. B. *J. Phys. Chem. C* **2009**, *113* (19), 8306−8312.

(20) El Kasmi, A.; Leopold, M. C.; Galligan, R.; Robertson, R. T.; Saavedra, S. S.; El Kacemi, K.; Bowden, E. F. *Electrochem. Commun.* **2002**, *4* (2), 177−181.

(21) (a) Araci, Z. O.; Runge, A. F.; Do Herty, W. J.; Saavedra, S. S. *J. Am. Chem. Soc.* **2008**, *130* (5), 1572−+. (b) Araci, Z. O.; Runge, A. F.; Doherty, W. J.; Saavedra, S. S. *J. Am. Chem. Soc.* **2011**, *133* (33), 13205−13205.

(22) (a) Ruzgas, T.; Wong, L.; Gaigalas, A. K.; Vilker, V. L. *Langmuir* **1998**, *14* (25), 7298−7305. (b) Gaigalas, A. K.; Ruzgas, T. *J. Electroanal. Chem.* **1999**, *465* (1), 96−101. (c) Li, L.; Meuse, C.; Silin, V.; Gaigalas, A. K.; Zhang, Y. Z. *Langmuir* **2000**, *16* (10), 4672−4677.

(23) (a) Brevnov, D. A.; Finklea, H. O.; Van Ryswyk, H. *J. Electroanal. Chem.* **2001**, *500* (1−2), 100−107. (b) Brevnov, D. A.; Finklea, H. O. *J. Electrochem. Soc.* **2000**, *147* (9), 3461−3466.

(24) Sagara, T.; Kato, N.; Kakashima, N. *J. Phys. Chem. B* **2002**, *106* (6), 1205−1212.

(25) Yamada, T.; Nango, M.; Ohtsuka, T. *J. Electroanal. Chem.* **2002**, *528* (1−2), 93−102.